Self-Consistent Solution of the Schr odinger and Poisson Equations Applied to Quantum Well Heterostructures

Technical Report · June 1998

CITATIONS
0

READS
123

4 authors, including:

Albert K. Henning
62 PUBLICATIONS **722** CITATIONS
SEE PROFILE

Charles E. Hembree
Sandia National Laboratories
47 PUBLICATIONS **145** CITATIONS
SEE PROFILE

Self-Consistent Solution of the Schrödinger and Poisson Equations Applied to Quantum Well Heterostructures

M. J. Hargrove and A. K. Henning

Thayer School of Engineering

Dartmouth College, Hanover, NH 03755

J. A. Slinkman

IBM Microelectronics, Essex Junction, VT 05452

C. E. Hembree

Texas Instruments, Dallas, TX

Subject Classification: 65PXX and 81C06

Running Head

Self-Consistent Solution of the Schrödinger and Poisson...

Mailing Address:

Michael Hargrove
Thayer School of Engineering
Hinman Box 8000
Dartmouth College
Hanover, NH 03766
hargrove@northstar.dartmouth.edu

Abstract

A novel numerical approach to solving Schrödinger's equation as applied to quantum well heterostructures is described. The quantum mechanical energy subbands, wave functions and charge density are calculated based on a two-directional fourth-order Runge-Kutta (RK4) algorithm. The algorithm is applied to well-defined quantum well structures. Results are compared with analytic solutions to ensure numerical accuracy. The approach is then extended to a self-consistent solution of the Schrödinger and Poisson equations applied to a $Si/Si_{1-x}Ge_x/Si$ heterostructure. The advantages of this method are compared to other solution techniques.

Introduction

The use of heterojunctions, or heterostructures, to improve the performance of semiconductor devices was first suggested by Shockley in 1951 [1]. At that time semiconductor technology was not mature enough to take advantage of such structures. Recent advances in epitaxial film growth, via molecular beam epitaxy (MBE) and ultra-high vacuum chemical vapor deposition (UHV/CVD), have enabled the deposition of single monolayers of semiconductor materials with unparalleled crystal perfection [2, 3]. These techniques enable ultra-thin structures to be grown with very sharp bandgap offsets, resulting in quantum confinement of carriers, not typically seen in classical device behavior [4]. Carrier confinement effects is a strong motivation for studying the quantum mechanical behavior of such structures, and thus requires the solution of Schrödinger's equation. For an even more accurate description of carrier confinement effects on device behavior, a fully self-consistent solution of the coupled Schrödinger and Poisson equations is required [5].

This paper presents a robust numerical solution of the Schrödinger equation applied to various quantum well configurations. The numerical results are validated by comparison to known analytic solutions for well-defined potential wells in terms of allowable energy levels and wave functions. The advantages of this numerical approach are described and compared to other solution techniques. A fully self-consistent numerical solution, coupling the Schrödinger and Poisson equations, is presented for the $Si/Si_{1-x}Ge_x/Si$ heterostructure. The iterative process of determining the wave function solutions of Schrödinger's equation from an initial potential distribution is described, followed by the calculation of the charge density which is used in Poisson's equation to arrive at the new potential distribution.

The motivation for such a calculation arises from the confinement of carriers within the quantum well formed by the sharp bandgap offsets between the various materials that form the heterostructure device. The following sections cover the solution technique employed to solve Schrödinger's equation, comparison to analytic solutions of well-defined quantum

wells, a description of the self-consistent solution of the coupled Schrödinger and Poisson equations applied to a $Si/Si_{1-x}Ge_x/Si$ heterostructure, and finally, a discussion of results and conclusion.

Numerical Solution of the Schrödinger Equation

The one-dimensional (1D), time-independent Schrödinger equation is given by

$$\frac{d^2\psi_n}{dz^2} + \frac{2m^*}{\hbar^2}\left[E_n - V(z)\right]\psi_n = 0 \tag{1}$$

where ψ_n is the wave function solution, E_n is the eigen-energy, V(z) is the spatially varying potential distribution, m^* is the electron (or hole) effective mass, and $\hbar$ is Planck's constant divided by 2π. The numerical solution of Eq. (1) can be found as far back as 1967 [6]. Since the 1D, time-independent Schrödinger equation is an ordinary differential equation (ODE), it can be solved by any of the standard methods for solving ODEs, e.g. Runge-Kutta and Numerov [7, 8]. Depending upon the complexities of the given quantum mechanical system, one approach may be favored over the others. For example, the Numerov method can provide a solution with an aggregate truncation error of order $O(\delta z)^8$ [9]. However, this method is only valid for homogeneous quantum well systems in which there can be no first-order derivative terms involving $\psi_n(z)$ or terms of the form $\frac{d}{dz}\left[\frac{1}{m^*(z)}\frac{d\psi_n(z)}{dz}\right]$. This can be a limitation since many state-of-the-art semiconductor heterostructures are formed from different materials with different effective masses, yielding spatially varying effective mass terms in the Schrödinger equation.

The fourth order Runge-Kutta (RK4) method takes advantage of a fourth order truncation error and eliminates the computation and evaluation of the derivatives required in a Taylor series method. The boundary conditions for the RK4 method can include both Dirichlet and Neumann conditions, typically specified at either the surface ($z = 0$), or the bulk ($z = z_{max}$, where z_{max} is the location of the boundary furthest from the surface). The RK4 method is also general enough to handle spatially varying material parameters.

Since the one-dimensional Schrödinger equation is an eigenvalue equation, standard numerical matrix eigenvalue solutions are also possible (e.g. Jacobi or Gauss-Seidel iterative algorithms). These techniques are viable for large linear systems. The limitation of such a numerical approach to the solution of complex quantum well heterostructures is the fact that only the eigenvalue solutions are obtained, with no ability to investigate continuum solutions, or solutions for $E > V(z)$. For room temperature device applications these continuum solutions will be important.

In this work, a modified version of the RK4 method of solution has been implemented, namely the *crossfire* method [10, 11]. As opposed to the standard RK4 method where the boundary conditions are specified at either the surface (z = 0) or the bulk (z = z_{max}), the boundary conditions for the *crossfire* method are specified at a patchpoint, z_{patch}. For single well systems the patchpoint can be arbitrarily defined anywhere inside the quantum well. For the arbitrary quantum well shown in Figure 1, the patchpoint is defined as

$$z_{patch} = \frac{z_2 + z_1}{2} \tag{2}$$

where z_1 and z_2 define the quantum well boundaries.

The *crossfire* method looks for solutions to Schrödinger's equation by choosing a starting energy value E_{min} and incrementing spatially from z = 0 to z = z_{patch} to find a corresponding wave function ψ_{LR} (where the subscript LR implies the left-to-right, or z = 0 to z = z_{patch}, solution). A right-to-left (RL) (z = z_{max} to z = z_{patch}) wave function, ψ_{RL}, is found for the same energy value. The two solutions are then matched at the patchpoint by the following boundary conditions

$$\psi_{LR}(z = z_{patch}) = \psi_{RL}(z = z_{patch}) \tag{3}$$

and

$$\frac{d\psi_{LR}}{dz}_{z=z_{patch}} = \frac{d\psi_{RL}}{dz}_{z=z_{patch}} \tag{4}$$

The final wave function solution is found by combining ψ_{RL} and ψ_{LR} which results in a wave function, $\psi(z)$, that is a combination of ψ_{RL} and ψ_{LR}, matched at z_{patch}. This

approach avoids any instability in the RK4 method that arises from a non-optimal choice of spatial discretization. Such instabilities, signified by the appearance of unbounded, lower eigen-energy solutions near the origin ($z = 0$), occured only for a one-way RK4 method, independent of direction. A typical example of this stability problem is shown in Figure 2.

By dividing Eq.(4) by Eq.(3), a determinant formulation for the boundary conditions is arrived at, namely,

$$\psi_{LR} \left.\frac{d\psi_{RL}}{dz}\right|_{z=z_{patch}} - \psi_{RL} \left.\frac{d\psi_{LR}}{dz}\right|_{z=z_{patch}} = 0 \tag{5}$$

which can be written as

$$\Xi = \begin{vmatrix} \psi_{LR} & \psi_{RL} \\ \frac{d\psi_{LR}}{dz} & \frac{d\psi_{RL}}{dz} \end{vmatrix} = 0 \tag{6}$$

The value of determinant Ξ indicates whether a bound state solution has indeed been found. If the determinant changes sign from one iteration to the next, then the eigenvalue solution, or bound state, has been bracketed.

The numerical solution of Schrödinger's equation based on the *crossfire* method first establishes the minimum energy from which to start the eigen-energy search. The first time through the energy loop the initial energy value is set to the lowest energy value of the system, typically $E_1 = E_{min}$. Schrödinger's equation is then solved for the given potential distribution V(z), at the specific energy E_1, resulting in wave function solutions, ψ^1_{RL} and ψ^1_{LR} (where supercript 1 indicates the first energy loop), which are matched at the patchpoint. Application of the boundary conditions yields the determinant, Ξ^1. The energy is then incremented to $E_2 = E_{min} + \Delta E$, where ΔE is typically 1 meV. Corresponding wave function solutions, ψ^2_{RL} and ψ^2_{LR}, are found and the resulting determinant, Ξ^2, is calculated. If the product of Ξ^1 and Ξ^2 is less than zero, indicating a sign change in the wave function solutions, then an eigen-energy has been bracketed between E_1 and E_2. A graphical interpretation of this is shown in Fig. 3 where the wave function solutions are shown to change sign at $z = z_{patch}$. The energy E_2, and value of the determinant Ξ^2, are then stored.

Once an eigen-energy is bracketed a binary-search method is used to refine the eigen-energy. The binary-search method divides the energy interval in two and proceeds to recalculate a new ψ_{RL}, ψ_{LR} and Ξ based upon the new energy, $\mathrm{E}_{new} = \frac{E_i + E_{i+1}}{2}$. The binary search continues until the energy halving is less than ϵ, where $\epsilon = 0.0001$ in these computations. The eigen-energy is further refined by implementing a Regula-Falsi search for the eigen-energy [8]. The Regula-Falsi search continues until the difference in energy, $\delta_E = \mathrm{E}_{new}$ - E_{old}, is less than ϵ_E, where ϵ_E can be set for arbitrary accuracy (e.g. $\epsilon_\mathrm{E} = 10^{-10}$).

If the number of iterations required to achieve a specified level of accuracy is exceeded, then the energy is incremented by ΔE and the process is repeated. For example, if the maximum number of iterations is specified as 200, then if the number of iterations in the eigen-energy search exceeds this value the search is stopped and the energy is incremented by ΔE in order to begin the calculation of a new solution point. Once $\delta_E < \epsilon_E$ then a bound state has been found. This process continues until the entire energy loop has been completed, e.g. $\mathrm{E} = \mathrm{E}_{max}$, or the energy exceeds the Fermi energy, E_F. In the latter case of $E > E_F$, we assume no additional bound states exist [12].

Optimizing the Patchpoint Location

The location of the patchpoint, z_{patch}, is very important in order to optimize the solution accuracy. For simple single quantum well configurations such as the finite square well and triangular well, the patchpoint need only be located somewhere within the well. Its location relative to the boundaries is unimportant, assuming it does not coincide with a nodal value of any given wave function solution. If z_{patch} does coincide with a wave function node (i.e. zero crossing of wave function), for example $\mathrm{z} = \mathrm{W}/2$ for the finite square well, then the solution may be discontinuous at $\mathrm{z} = \mathrm{z}_{patch}$, though the eigen-energies will continue to be accurate. If wave function nodal value locations are unknown, more than one iteration of the problem may be required to yield a smooth, continuous wave function solution.

For more complicated quantum well systems, e.g. $Si/Si_{1-x}Ge_x/Si$ heterostructures discussed in subsequent sections, more knowledge of the particular quantum well configuration and bias conditions is helpful in optimizing the patchpoint location. For example, if the energy band configuration for a given bias condition results in only the $Si_{1-x}Ge_x$ quantum well being populated, with few states in the Si surface well (see Figure 11), then the patchpoint should be located inside the $Si_{1-x}Ge_x$ well.

Comparison to Analytic Results

Finite Square Well Application

The numerical solution of Schrödinger's equation is validated by comparing the numerical results of a finite square well to the analytic solution. The analytic solution of a given finite square well can be found in any standard quantum mechanics text [13]. Typically, the solution is determined graphically based upon the boundary conditions that the wave function solutions, and their first derivative, match at the well boundary. The finite square well shown in Figure 4, with W = 10 nm and V_o = -0.2 eV, results in eight bound states with eigen-energies given in Table 1. The total number of bound states in a finite square well of depth V_o and width W can be found from [14]

$$Number of States = 1 + Int\left[\left(\frac{2m^* V_o W^2}{\pi^2 \hbar^2}\right)^{1/2}\right] \tag{7}$$

where Int[x] indicates the integer part of x. For the square well described above, Eq. (7) also yields eight eigen-energies. The numerical values of these eight eigen-energies are shown in Table 1 along with the analytic results.

The numerical results are in excellent agreement with the analytic results, with a maximum error of less than 0.1% for the ground state and first three excited states. The highest eigen-energy state results in an error of 0.28%. The resulting percent error are calculated relative to the bottom of the quantum well, V_o. That is, we choose to define the position

n	$E_n(analytical)$ (eV)	$E_n(numerical)(eV)$	Error (%)
1	-0.196817	-0.196826	0.0045
2	-0.187286	-0.187323	0.0185
3	-0.171460	-0.171544	0.0420
4	-0.149444	-0.149595	0.0755
5	-0.121422	-0.121661	0.1195
6	-0.087737	-0.088089	0.1760
7	-0.049149	-0.049632	0.2420
8	-0.008503	-0.009069	0.2830

Table 1: Eigen-energies of finite square well of width W = 100 Å and depth of V_o = -0.2 eV, determined analytically and numerically.

of the energy level E_n, relative to the bottom of the quantum well V_o, as (E_n - V_o), which gives the difference in energy between E_n and V_o. The relative error between the analytical results and the numerical results is then defined by

$$Error(\%) = \frac{|[E_n(analytical) - V_o] - [E_n(numerical) - V_o]|}{V_o} = \frac{|[E_n(analytical) - E_n(numerical)]|}{V_o} \quad (8)$$

The larger error for the higher lying states is related to the increased energy separation between the states as n increases. This will tend to degrade the accuracy of the numerical solution. In actual device operation, however, the higher lying bound states do not get populated due to the Fermi energy location. Therefore, in most applications only the first two or three bound states are of significant importance. The first three corresponding wave function solutions for this example are shown in Fig. 5. The basic shapes of the wave functions are sinusoidal inside the quantum well and decaying exponentials outside the well, as expected from the analytical solution [13].

n	E_n(analytical) (eV)	E_n(numerical) (eV)	Error (%)
1	-0.1424539	-0.152067	0.2200
2	-0.0987644	-0.109143	0.0762
3	-0.0631652	-0.074195	0.0420
4	-0.0317343	-0.043546	0.0282
5	-0.0030132	-0.016091	0.0210

Table 2: Eigen-energies of triangular potential well of width W = 100 Å and depth V_o= -0.2 eV, determined analytically and numerically.

Triangular Square Well Application

The numerical solution of the Schrödinger equation for the triangular potential well shown in Figure 6 with W = 10 nm and potential distribution given by

$$V_{triangle well}(z) = V_o\,(zF - 1) \tag{9}$$

results in five bound states. Here, F is the slope of the potential well distribution. For a triangular well with V_o = -0.2 eV, the slope of the potential well distribution is F = 2.0 x $10^{\,5}$ eV/cm. The resulting eigen-energies are shown in Table 2 compared to the analytic results.

The numerical results compare reasonably well for all of the eigen-energies. The smaller percent error for the higher lying bound states is due to the fact that the higher lying states are closer together than the lower lying states. Therefore, the relative error between the analytic solution and the numerical solution will be smaller. This result is opposite to the finite square well case. Another component of error is due to the numerical solution assuming a finite well width, while the analytic solution assumes the well goes on forever with a constant slope.

The corresponding wave function solutions for this example are shown in Fig. 7. These wave function solutions show similar behavior to the analytically derived wave function solutions found in [15], which are Airy functions.

Coupling the Schrödinger and Poisson Equations Numerically

In order to calculate the self-consistent potential of a given quantum heterostructure system, Poisson's equation must be solved to determine the electrostatic potential. Poisson's equation relates the potential to the charge density distribution in the semiconductor heterostructure. The solution of Schrödinger's equation provides the eigen-energies and the corresponding wave functions. The wave functions are used in the calculation of the charge density distribution. The charge density is calculated by summing the square of the wave function solutions at each spatial increment and over all the populated bound states, and multiplying this quantity by the number of carriers in each bound state (subband). The electron charge density n(z) is given by

$$n(z) = \sum_n N_n \ |\psi_n(z)|^2 \tag{10}$$

where N_n is the number of electrons per subband. This quantity is determined from the two-dimensional density of states function, $g_{2D}(E)$, given by [14]

$$g_{2D}(E) = \frac{m^*}{\pi\hbar^2} \tag{11}$$

The subband occupation density, N_n, is given by the integration of $g_{2D}(E)$ weighted by the Fermi-Dirac distribution f(E). The Fermi-Dirac distribution function specifies the probability that a given subband energy level, E_n, is occupied by an electron, at a specific temperature [13], and is given by

$$f(E) = \frac{1}{1 + \exp\left[(E_n - E_F)/k_B T\right]} \tag{12}$$

N_n is then given by

$$N_n = \int_{E_n}^{\infty} g_{2D}(E)\, f(E)\, dE \tag{13}$$

The resulting integration yields

$$N_n = \frac{k_B T m^*}{\pi \hbar^2}\, \ln\left[1 + \exp\left(\frac{E_F - E_n}{k_B T}\right)\right] \tag{14}$$

where k_B is Boltzmann's constant and T is temperature.

The Poisson equation is given by

$$\frac{d^2 V(z)}{dz^2} = -\frac{4\pi e^2}{\epsilon}\left(n(z) - p(z) + N_a^- - N_d^+\right) \tag{15}$$

where $n(z)$ is the electron charge distribution, $p(z)$ is the hole distribution, N_a^- is the ionized acceptor concentration, and N_d^+ is the ionized donor concentration. The dielectric constant, ϵ, is assumed to be spatially constant, and e is the electronic charge. Knowing the charge density $n(z)$ (neglecting $p(z)$ if we consider electrons) and the background doping concentration N_a^- and N_d^+ (which can also varies with position), Poisson's equation is solved by a standard finite difference routine. The second order differential $\frac{d^2V(z)}{dz^2}$ is rewritten, assuming a centered-difference approach and a uniform one-dimensional mesh, as

$$\frac{d^2 V(z)}{dz^2} = \frac{V_{i+1} - 2V_i + V_{i-1}}{\Delta z^2} \tag{16}$$

where V_i is the potential at the i^{th} node of a one-dimensional mesh representing the quantum well of interest, and Δz is the mesh nodal spacing. Substituting Eq.(16) into Eq.(15) yields

$$V_{i+1} - 2V_i + V_{i-1} = \frac{-4\pi e^2 \Delta z^2}{\epsilon}\left[n(z) - p(z) + N_A^- - N_D^+\right] \tag{17}$$

This equation relates the potential at the i^{th} node to the potential at the i^{th}+1 and i^{th}-1 nodes, as well as the node spacing Δz and the charge density. The boundary conditions for the solution of Poisson's equation are given by

$$V(z)\mid_{z=0} = V_o \tag{18}$$

and

$$\frac{dV(z)}{dz} \mid_{z=z_{max}} = 0 \tag{19}$$

These conditions force the self-consistent solution to be equal to the original surface potential V(z=0) = V_o, and also require the electric field to be zero at z = z_{max}. The finite difference algorithm must then account for Dirichlet boundary conditions at z = 0, and Neumann boundary conditions at z = z_{max}. Equation (17) can be written in matrix form as

$$\begin{bmatrix} 1 & -0.5 & 0 & \cdots & 0 & 0 \\ -0.5 & 1 & -0.5 & \cdots & 0 & 0 \\ & & \ddots & & & \\ 0 & 0 & 0 & \cdots & 1 & -0.5 \\ 0 & 0 & 0 & \cdots & -0.5 & 1 \end{bmatrix} \begin{bmatrix} V_1 \\ V_2 \\ \vdots \\ V_{n-1} \\ V_n \end{bmatrix} = \begin{bmatrix} -\Delta z^2 \rho(z) + V_o \\ -\Delta z^2 \rho(z) \\ \vdots \\ -\Delta z^2 \rho(z) \\ -\frac{3}{2}\Delta z^2 \rho(z) \end{bmatrix} \tag{20}$$

where $\rho(z) = -\frac{4\pi e^2}{\epsilon}\left[n(z) - p(z) + N_A^- - N_D^+\right]$. This matrix equation is solved by a standard tridiagonal matrix solver.

In order to determine if the calculated potential distribution V(z) is self-consistent, the error between the new and old potentials must be calculated. V_{new}(z) must be mixed with the old V_{old}(z) in order to ensure convergence of the algorithm. If V_{new}(z) is simply substituted back into Schrödinger's equation, then the iterative process of calculating the wave function solutions, charge density, and resulting potential distribution has been shown not to converge [16]. The mixing of the old and new potential distribution is accomplished by implementing the extrapolated convergence-factor method [16]. The mixing algorithm is schematically shown in Figure 8. The equation representing the mixing algorithm is given by

$$V(z) = V_{in}^{i+1}(z) = V_{in}^{i}(z) + f_{in}^{i+1}\left[V_{out}^{i}(z) - V_{in}^{i}(z)\right] \tag{21}$$

The value of f_{in}^{i+1} is chosen between 0.05 and 0.1. This factor represents the mixing fraction of new and old potentials. If f_{in}^{i+1} is too large then the algorithm may run quickly but can

also diverge. If it is too small, then the convergence is slow. In this work f_{in}^{i+1} is typically set to 0.05. It is also possible to vary f_{in}^{i+1} from iteration to iteration [16]. Once the mixing is complete, the self-consistent solution of the i^{th} iteration is compared to the $(i\text{-}1)^{th}$ solution by calculating

$$\chi^2 = \sum_z \left[\frac{\left(V_{sc}^i(z) - V_{sc}^{i-1}(z)\right)^2}{V_o^2} \right] \tag{22}$$

If $\chi^2 \leq 10^{-3}$ then the self-consistent solution has been found. A detailed flow diagram of the self-consistent calculation is shown in Figure 9.

Self-Consistent Solution of the Schrödinger-Poisson Equations Applied to $Si/Si_{1-x}Ge_x/Si$ Heterostructures

The $Si/Si_{1-x}Ge_x/Si$ heterostructure is expected to play a major role in Si-based heterostructural technologies of the future, including both bipolar and field-effect transistor (FET) technologies. This is due to the structural and electrical compatibility of Ge and Si, and also the sophistication of Si-based processing in general (e.g. oxide growth, passivation, etc.). Although the applications of such heterostructures are many, the focus of this work is in calculating the energy subbands of an FET-like structure with a $Si_{1-x}Ge_x$ channel region.

By incorporating a $Si_{1-x}Ge_x$ layer in the channel region of an FET device, the intrinsic mobility increases due to a reduction in surface scattering. The reduced surface scattering is achieved by incorporating the $Si_{1-x}Ge_x$ layer a few nanometers away from the Si/SiO_2 interface where carrier scattering reduces channel mobility.

The $Si/Si_{1-x}Ge_x/Si$ energy band under study is shown in Figure 11. This energy band configuration will be found in a p-channel SiGe FET under inversion conditions. In this case, holes will populate the quantum well formed by the Si/SiO_2 interface and also the $Si/Si_{1-x}Ge_x/Si$ quantum well. The silicon substrate doping level is set at $N_a = 10^{17}$ cm^{-3}, the surface potential is set at V_o = -0.2eV, and room temperature operation (T = 300 K)

n	E_n
1	-0.236375
2	-0.219000
3	-0.199062
4	-0.173875
5	-0.165250
6	-0.145000

Table 3: Eigen-energies of $Si/Si_{1-x}Ge_x/Si$ heterostructure.

is assumed. The different effective masses and dielectric constants of Si and $Si_{1-x}Ge_x$ are accounted for by changing the values of m^*_{Si} and ϵ_{Si} to m^*_{SiGe} and ϵ_{SiGe} as a function of spatial location. The bandgap offset between the $Si_{1-x}Ge_x$ layer and the Si substrate is set at 0.15 eV, corresponding to roughly a 20 % mole fraction of Ge present in the alloy (e.g. x = 0.2).

The resulting eigen-energies for holes in the $Si_{1-x}Ge_x$ quantum well and the Si surface channel are shown in Table 3. The accompanying wave function solutions are shown in Figure 12. For this example, most of the wave function solutions are localized within the boundaries of the quantum well, while the two highest lying states are in the Si surface channel, indicating that some of the associated charge density will reside in the Si surface channel.

As V_o becomes increasingly negative, the Fermi energy rises higher in the surface channel well, and more of the wave functions begin to penetrate into the Si surface channel region. As a consequence, a finite amount of charge will tunnel quantum mechanically from the $Si_{1-x}Ge_x$ well into the surface channel well, where the carriers have lower mobility. As V_o continues to increase, a larger percentage of carriers find their way into the Si surface channel well. This effect is shown in Figure 13 where the calculated charge density

is plotted versus distance as a function of V_o.

Since optimal device performance is dependent upon the relative distribution of charge between the $Si_{1-x}Ge_x$ quantum well and the Si surface channel, the ability to simulate the charge distribution within a SiGe FET is extremely advantageous. By varying the location of the $Si_{1-x}Ge_x$ quantum well relative to the surface channel, one can study the effects on charge distribution and ultimately understand the optimal location of the $Si_{1-x}Ge_x$ alloy in a SiGe FET.

Conclusion

A robust numerical algorithm, based on a two-directional Fourth-Order Runge Kutta solution technique, is presented for solving the 1D, time-independent Schrödinger equation as applied to semiconductor quantum well heterostructures. The numerical accuracy has been verified by comparison to well defined quantum well configurations with analytic solutions. The advantages of this numerical approach compared to other viable numerical algorithms, has been discussed. The numerical approach results in accurate solutions, and offers the capability of extensions to more complex problems, including the ability to solve systems with spatially varying effective mass and dielectric constant.

The self-consistent solution has been applied to $Si/Si_{1-x}Ge_x/Si$ heterostructure FETs, which offer the advantages of heterostructures with the processing maturity of Si. The applications of such structures are many. However, our focus has been on SiGe FETs. The self-consistent solution has provided a means to investigate the effect of charge density distribution in a SiGe MOSFET structure. As the band bending increases, the ratio of Si channel charge to SiGe well charge can be minimized by incorporating a SiGe alloy with smaller bandgap, resulting in a larger band offset between the Si and $Si_{1-x}Ge_x$ layers. Variations in other SiGe FET parameters, such as the Si channel thickness and doping density, and their effect on the charge distribution, can now be studied with the necessary

quantum mechanical effects included.

References

[1] W. Shockley, U.S. Patent 2569347, 25 September 1951.

[2] H. C. Casey, Jr., A. Y. Cho and P. A. Barnes, *IEEE J. Quantum Electron.*, **QE-11**, 467 (July 1975).

[3] E. Kasper and J. F. Luy, *Microelectronics Journal*, **22**, 5 (1991).

[4] J. C. Bean, *IEEE Proceedings*, **80**, 571 (April 1992).

[5] S. E. Laux and F. Stern, *Appl. Phys. Lett.*, **49** (2), 91 (1986).

[6] J. Blatt, *Jour. Comp. Phys.*, **1**, 382 (1967).

[7] D. R. Hartree, *Numerical Analysis*, 2nd Ed., Oxford University Press, England, 1958.

[8] R. L. Burden and J. D. Faires, *Numerical Analysis*, 4th Ed., PWS-KENT Publishing Co., Boston, MA, 1989.

[9] P. C. Chow, *Amer. J. Phys.*, **40**, 730, May 1972.

[10] W. H. Press, *et al.*, *Numerical Recipes in C*, Cambridge University Press, 1988.

[11] C. Hembree, Ph.D.Dissertation, University of Oklahoma, Norman, OK (1994).

[12] Here we assume no continuum states. Actually, the Fermi distribution of carriers will have a tail that extends beyond E_F such that solutions may exist for $E > E_F$.

[13] R. L. Liboff, *Introductory Quantum Mechanics*, 2nd Edition, Addison-Wesley, Reading, MA, 1992.

[14] C. Weisbuch and B. Vinter, *Quantum Semiconductor Structures*, Academic Press Inc., New York, 1991.

[15] T. Ando, A. B. Fowler and F. Stern, *Rev. Mod. Phys.*, **54**, (April 1982).

[16] F. Stern, *J. Comp. Physics*, **6**, 56 (1970).

Figure Captions

Figure 1. Arbitrary quantum well describing the patchpoint location.

Figure 2. A typical example of the instability of a one-directional RK4 solution to Schrödinger's equation. Here the lowest lying eigen energy *blows up* due to non-optimal spatial discretization.

Figure 3. Illustration of a sign change in the wave function ψ, at two different energy values E_i and E_{i-1}, resulting in a sign change in the determinant Ξ. This indicates that the eigen-energy is bracketed between E_i and E_{i-1}.

Figure 4. Finite square well of width W = 10 nm and depth of V_o = -0.2 eV.

Figure 5. Numerical wave function solutions for a finite square well of width W = 10 nm and depth of V_o = -0.2 eV.

Figure 6. Triangular potential well of width W = 10 nm and depth of V_o = -0.2 eV.

Figure 7. Numerical wave function solutions for a triangular potential well of width W = 10 nm and depth of V_o = -0.2 eV.

Figure 8. Schematic representation of the extrapolated convergence-factor method.

Figure 9. Flow diagram of complete self-consistent calculation.

Figure 10. Si/$Si_{1-x}Ge_x$/Si FET structure.

Figure 11. Si/$Si_{1-x}Ge_x$/Si energy band for an p-channel SiGe FET biased in inversion.

Figure 12. Si/$Si_{1-x}Ge_x$/Si wave function solutions for V_o = 0.2 eV.

Figure 13. Charge density vs distance, as a function of V_o, for a Si/$Si_{1-x}Ge_x$/Si heterostructure (T = 300 K).

Figure 1:

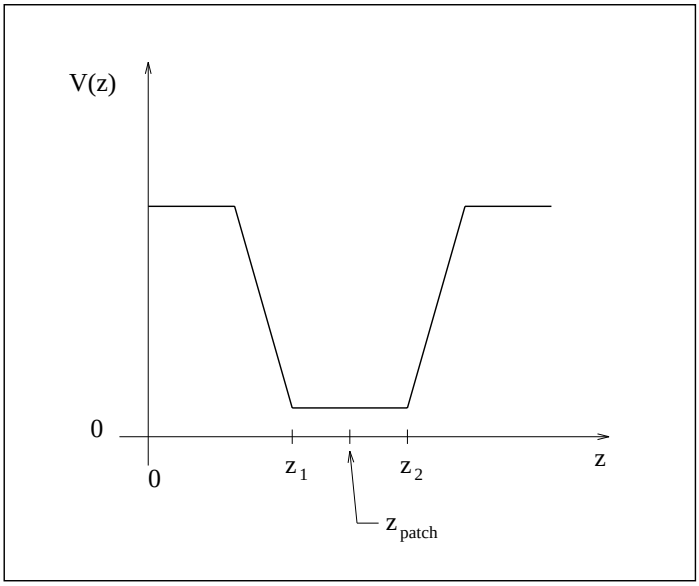

Figure 2:

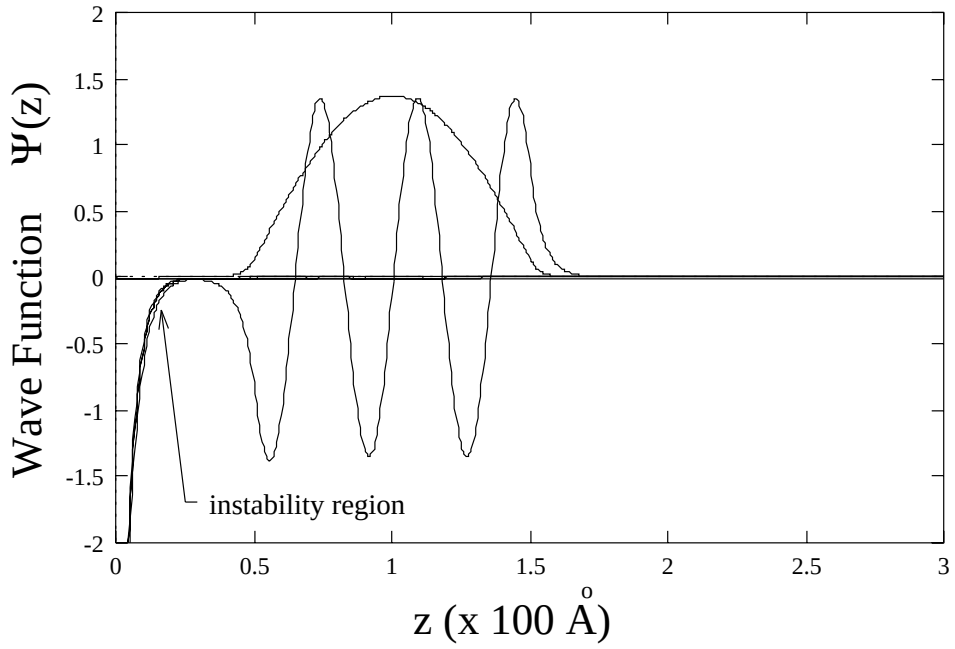
Wave Function Ψ(z)
2
1.5
1
0.5
0
-0.5
-1
-1.5
-2
0
0.5
1
1.5
2
2.5
3
instability region
z (x 100 Å)

Figure 3:

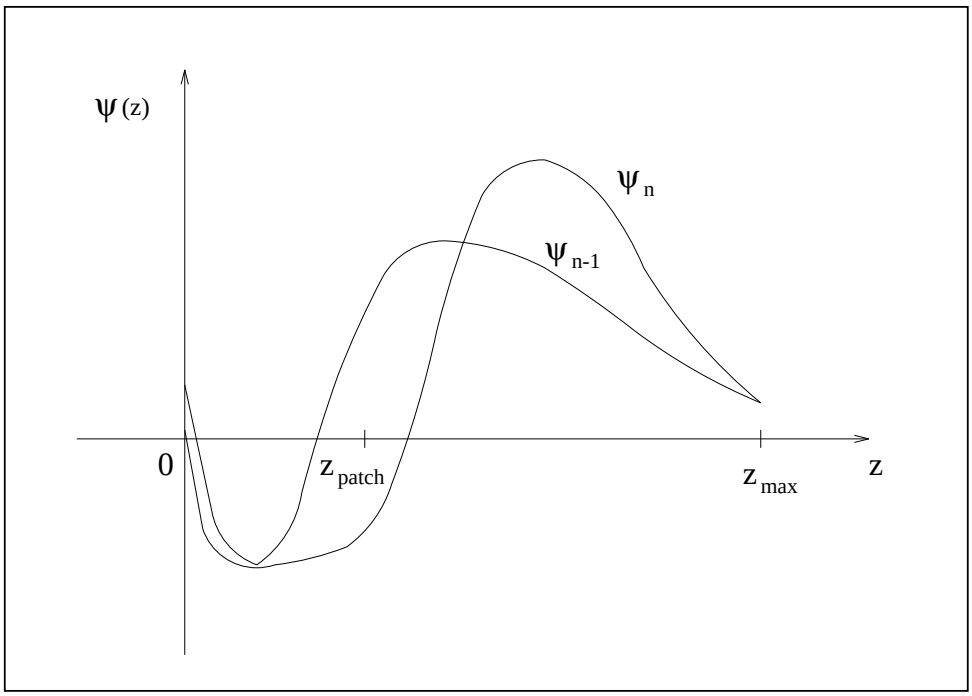

Figure 4:

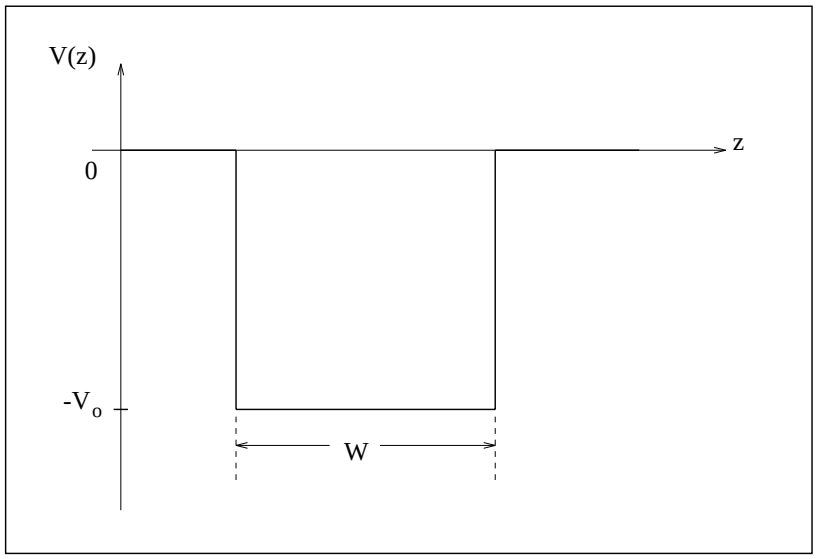

Figure 5:

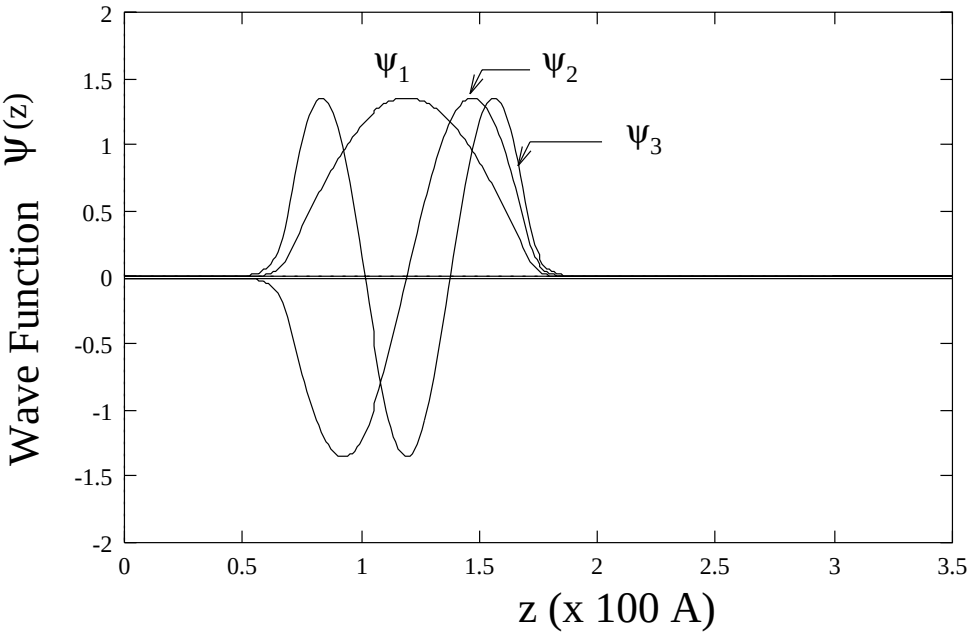
Wave Function ψ(z)
z (x 100 A)
ψ1
ψ2
ψ3
2
1.5
1
0.5
0
-0.5
-1
-1.5
-2
0
0.5
1
1.5
2
2.5
3
3.5

Figure 6:

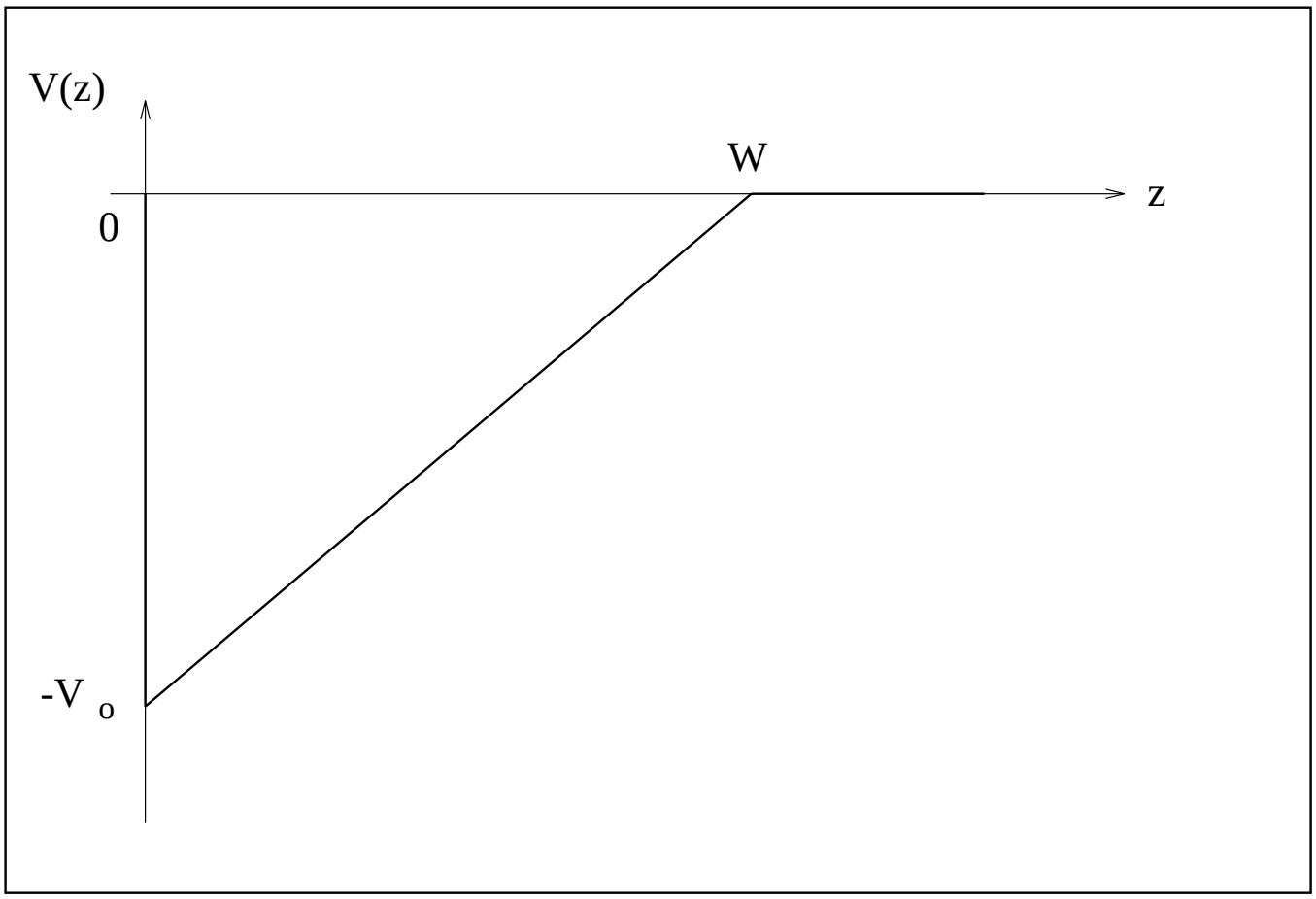

Figure 7:

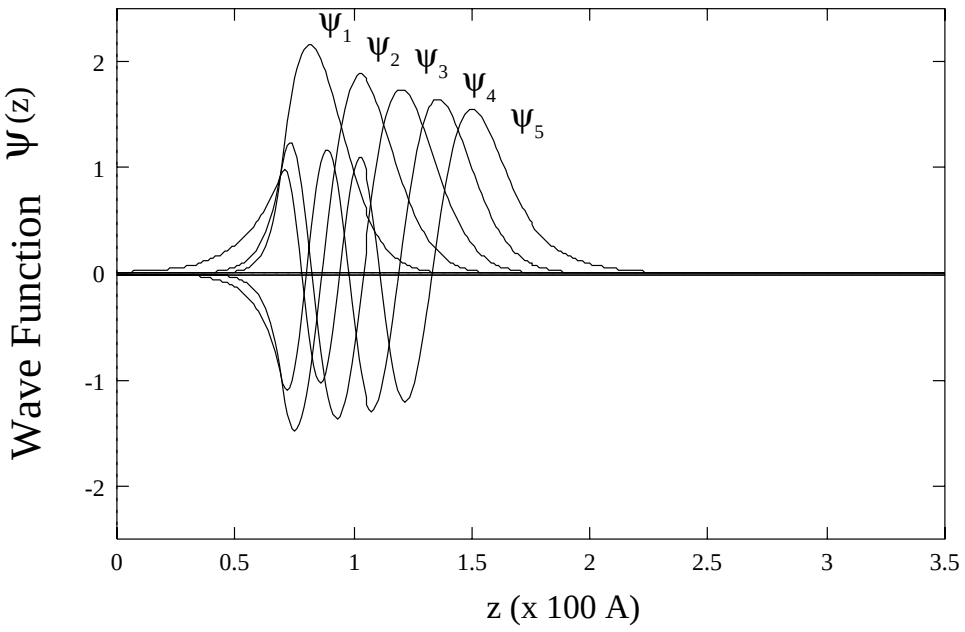

Figure 8:

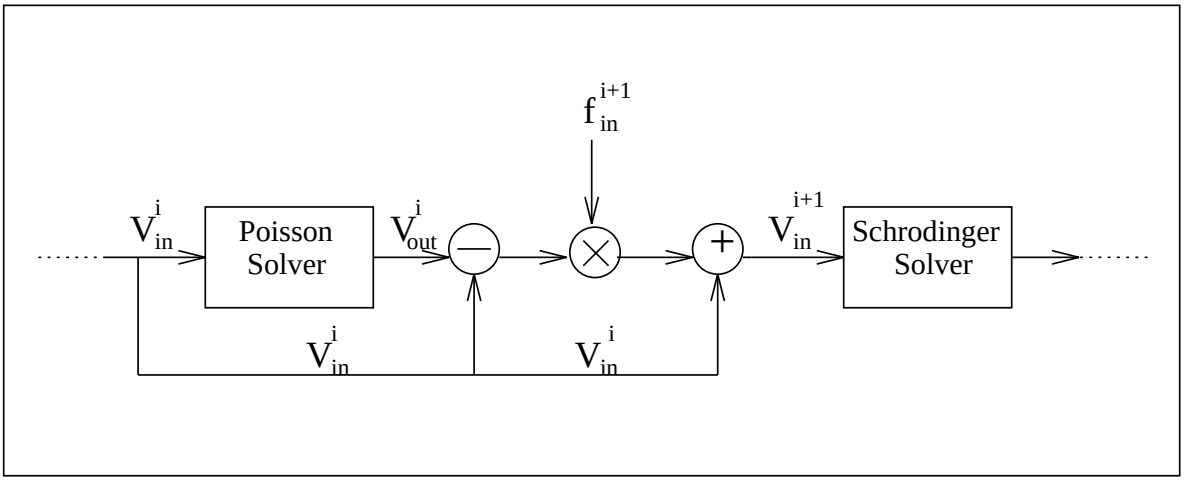
f in i+1
V in i
Poisson Solver
V out i
V in i+1
Schrodinger Solver
V in i
V in i

Figure 9:

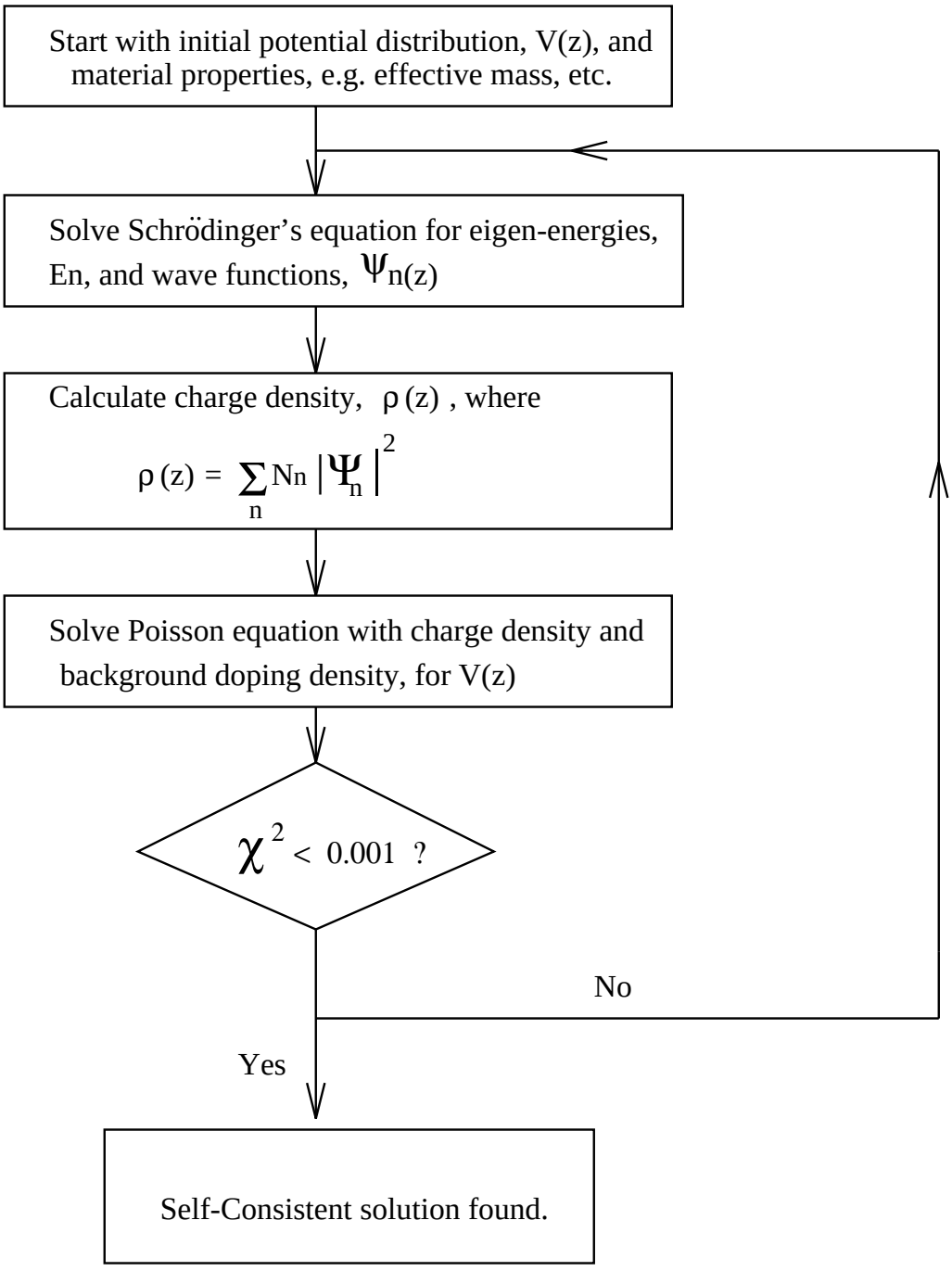
Start with initial potential distribution, V(z), and material properties, e.g. effective mass, etc.
Solve Schrödinger's equation for eigen-energies, En, and wave functions, Ψn(z)
Calculate charge density, ρ(z), where
ρ(z) = Σn Nn |Ψn|2
Solve Poisson equation with charge density and background doping density, for V(z)
χ2 < 0.001 ?
No
Yes
Self-Consistent solution found.

Figure 10:

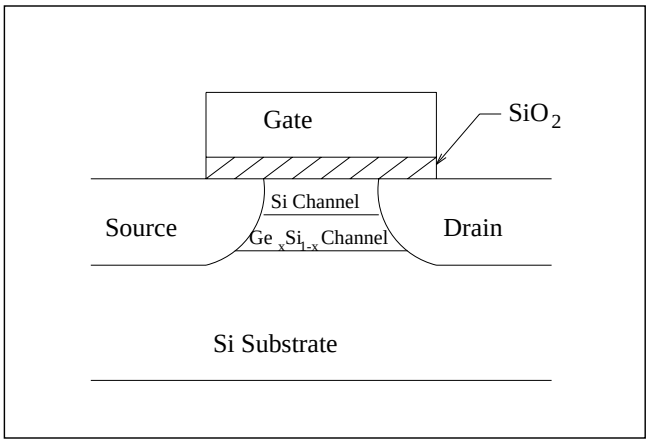

Figure 11:

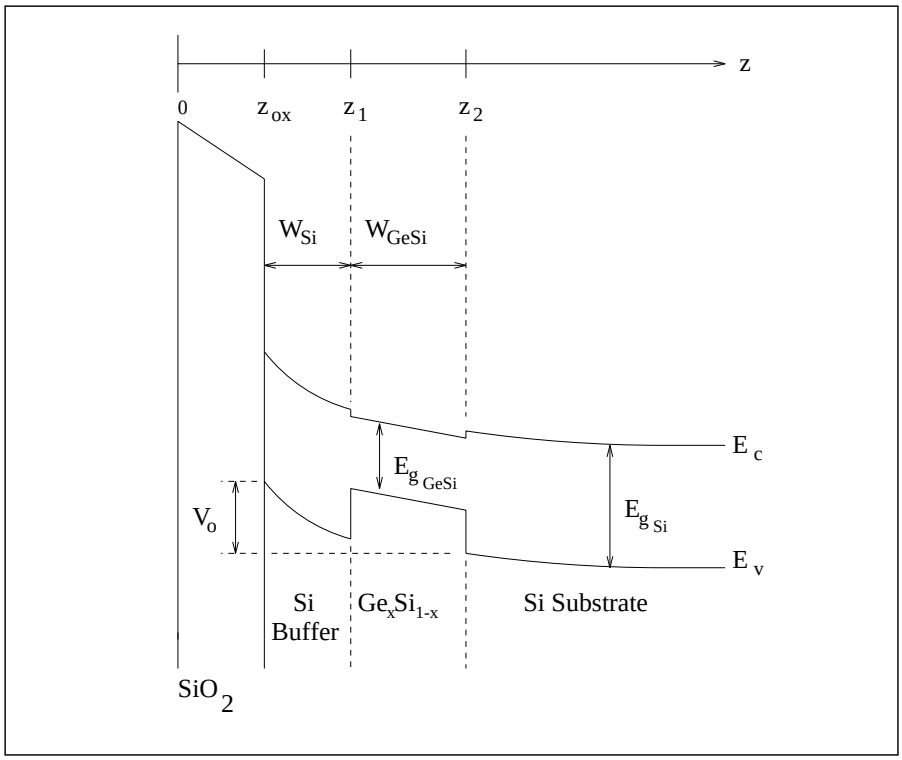

Figure 12:

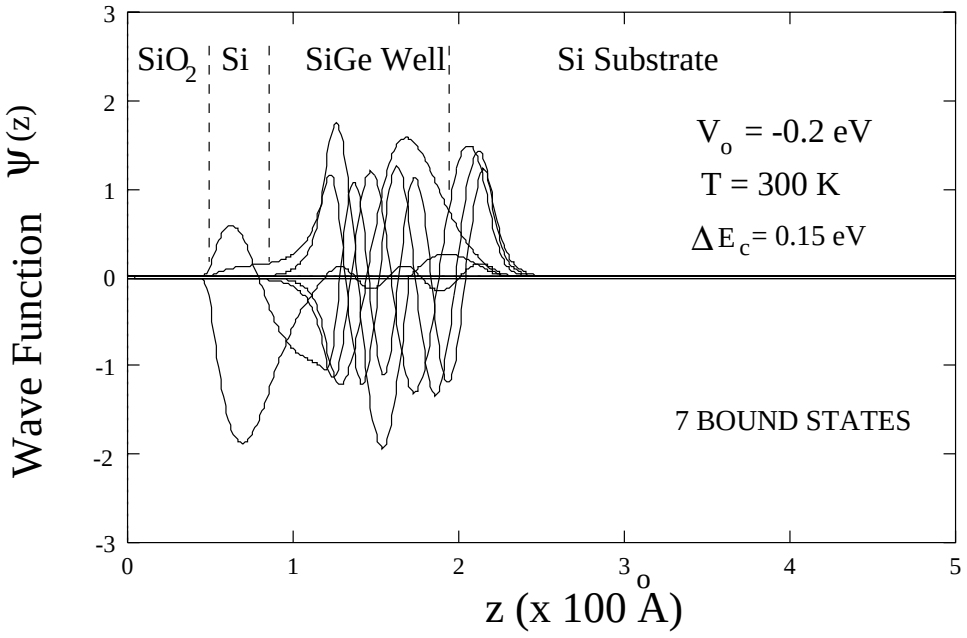
SiO2
Si
SiGe Well
Si Substrate
Vo = -0.2 eV
T = 300 K
ΔEc = 0.15 eV
7 BOUND STATES
Wave Function ψ(z)
z (x 100 Å)
3
2
1
0
-1
-2
-3
0
1
2
3
4
5

Figure 13: